nature biotechnology

Protein microarrays with carbon nanotubes as multicolor Raman labels

Zhuo Chen[1,4], Scott M Tabakman[1,4], Andrew P Goodwin[1], Michael G Kattah[2], Dan Daranciang[1], Xinran Wang[1], Guangyu Zhang[1], Xiaolin Li[1], Zhuang Liu[1], Paul J Utz[2], Kaili Jiang[3], Shoushan Fan[3] & Hongjie Dai[1]

The current sensitivity of standard fluorescence-based protein detection limits the use of protein arrays in research and clinical diagnosis. Here, we use functionalized, macromolecular single-walled carbon nanotubes (SWNTs) as multicolor Raman labels for highly sensitive, multiplexed protein detection in an arrayed format. Unlike fluorescence methods, Raman detection benefits from the sharp scattering peaks of SWNTs with minimal background interference, affording a high signal-to-noise ratio needed for ultra-sensitive detection. When combined with surface-enhanced Raman scattering substrates, the strong Raman intensity of SWNT tags affords protein detection sensitivity in sandwich assays down to 1 fM—a three-order-of-magnitude improvement over most reports of fluorescence-based detection. We use SWNT Raman tags to detect human autoantibodies against proteinase 3, a biomarker for the autoimmune disease Wegener's granulomatosis, diluted up to 10^7-fold in 1% human serum. SWNT Raman tags are not subject to photobleaching or quenching. By conjugating different antibodies to pure ^{12}C and ^{13}C SWNT isotopes, we demonstrate multiplexed two-color SWNT Raman-based protein detection.

Several methods can detect proteins for proteomic and clinical diagnostic applications. These include enzyme-linked immunosorbent assays (ELISAs), fluorescence-based protein microarrays[1], electrochemistry[2], label-free optical methods[3,4], surface-enhanced Raman scattering (SERS)[5–7], microcantilevers[8], quantum dots[9,10] and nanotube-[11,12] or nanowire-based[13] field-effect transistors. Among these, protein microarrays[14,15] are the most common methods providing high-throughput, multiplexed protein detection for a range of applications[14,16,17]. Typically, undesirable background interference or autofluorescence resulting from assay reagents and materials limits the sensitivity of protein arrays based on fluorophore tags to ~1 pM[18]. Increasing the sensitivity of protein detection in arrayed format could enhance the capability of this technology for proteomics research. Moreover, identification of soluble biomarkers for many diseases has increased clinical demands for high sensitivity and selectivity in protein detection to facilitate minimally invasive risk assessment, early-stage disease diagnosis and monitoring of responses to therapeutic interventions[19]. In addition to improving detection sensitivity, protein sensor platforms for diagnosis and research applications would benefit greatly from expanded dynamic ranges, which allow more samples to be compared simultaneously with the same standard set, thereby increasing throughput and reducing the quantity of reagents required.

At least two methodologies under development show particular promise for highly sensitive protein detection in research and clinical applications. Although label-free, nanowire-based transistors[13] demonstrate femtomolar sensitivity, this sensitivity is limited to samples in pure water or low-salt solutions, and cannot be achieved in serum or other physiological fluids. The second strategy, amplified detection based upon multifunctional nanoparticles, has even greater sensitivity[10] but requires multiple reagents and is very time consuming. Our methodology, based upon Raman scattering, has simpler requirements, may be easily multiplexed and exhibits high sensitivity in clinically relevant samples over the nM to fM range.

The SERS effect provides the potential for rapid, high-throughput, sensitive protein detection. Although SERS has been applied for immobilized protein detection by coupling small Raman-active dyes to gold nanoparticles functionalized by ligands[5,6], the utility of these sensors is limited by the weak intensities of typical Raman labels, owing to their small Raman scattering cross-sections[20]. As a result, sensitivity is not quantitative[5], or is limited to the nM range[5], which does not compare favorably with fluorescence methods. For high-sensitivity Raman sensing with dye molecules[7], long acquisition times are needed and molecules are subject to degradation, resulting from laser radiation.

In contrast, SWNTs are ideal labels for SERS-based protein detection. SWNTs have a unique one-dimensional structure and exhibit distinct electrical and spectroscopic properties, including strong and simple resonance Raman signatures. SWNTs possess enormous Raman scattering cross-sections ($\sim 10^{-21}$ cm^2 sr^{-1} molecule^{-1}), have simple and tunable spectra and are more stable than other organic Raman labels[21,22]. Various schemes have been explored to develop

[1]Department of Chemistry and Laboratory for Advanced Materials, Stanford University, 333 Campus Drive, Mudd Building, Room 121, Stanford, California 94305, USA. [2]School of Medicine, Stanford University, 269 Campus Drive, Stanford, California 94305, USA. [3]Department of Physics, Tsinghua-Foxconn Nanotechnology Research Center, Tsinghua University, Beijing 100084, China. [4]These authors contributed equally to the work. Correspondence should be addressed to H.D. (hdai@stanford.edu).

Received 4 June; accepted 18 September; published online 26 October 2008; doi:10.1038/nbt.1501

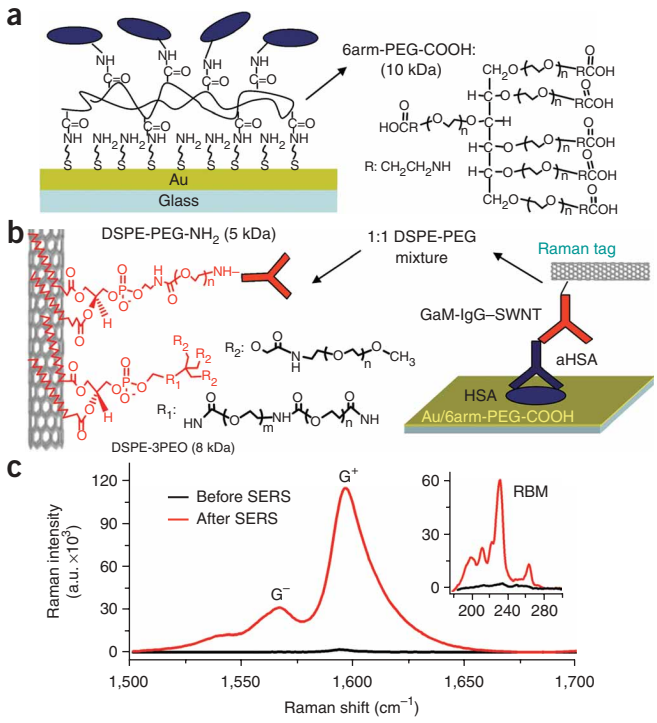

Figure 1 Carbon nanotubes as Raman labels for protein microarray detection. (**a**) Surface chemistry used to immobilize proteins on gold-coated glass slides for Raman detection of analytes by SWNT Raman tags. A self-assembled monolayer of cysteamine on gold was covalently linked to six-arm, branched poly(ethylene glycol)-carboxylate (6arm-PEG-COOH, right) to minimize nonspecific protein binding. Terminal carboxylate groups immobilize proteins. (**b**) Sandwich assay scheme. Immobilized proteins in a surface spot were used to capture an analyte (antibody) from a serum sample. Detection of the analyte by Raman scattering measurement was carried out after incubation of SWNTs conjugated to goat anti-mouse antibody (GaM-IgG–SWNTs), specific to the captured analyte. SWNTs were functionalized by (DSPE-3PEO) and (DSPE-PEG_{5000}-NH2) (left). (**c**) Raman spectra of the SWNT G mode and radial breathing mode (RBM, inset) regions before and after SERS enhancement.

SWNTs for chemical, biological and medical applications[23–27]. Although carbon nanotubes have been used as *in vivo*[28] and *in vitro*[29] optical probes for biological imaging, their potential as Raman tags for highly sensitive detection applications has not been explored.

We have prepared biocompatible, highly selective SWNT-immunoglobulin G conjugates for *in vitro* protein detection. Well-known self-assembly chemistry for protein immobilization was combined with our methodology for obtaining surface-enhanced Raman scattering over large areas. Coupled with the benefits of Raman scattering detection, these SWNT-based macromolecular Raman labels permit highly sensitive and selective arrayed protein detection. For systems with high-affinity interactions, sensitivity is 1,000-fold greater than fluorescence over seven to eight decades of dynamic range. We demonstrate detection of the clinically relevant human-autoimmune-disease biomarker anti–proteinase 3 in human serum diluted 10^7-fold. Isotopic SWNTs provide multiple-color SWNT Raman labels for multiplexed sensing, requiring only a single excitation source.

RESULTS

Assay design for protein detection by SWNT Raman tags

To highly water-soluble, short (~50–150 nm; **Supplementary Fig. 1** online), macromolecular SWNTs functionalized with PEGylated phospholipids[26], we conjugated a secondary antibody, goat anti-mouse immunoglobulin G (GaM-IgG), which mediated specific binding of SWNT tags to mouse antibodies (**Fig. 1**). Protein immobilization on substrates was performed in arrayed fashion, by either covalent attachment to gold-coated glass or on commercial microarray slides by standard robotic spotting. We developed a novel six-arm, branched, carboxylate-terminated PEG. When grafted onto gold-coated surfaces for protein immobilization (**Fig. 1a**), this afforded excellent protein attachment and substantially helped to overcome nonspecific binding. Proteins, such as polyclonal mouse IgG or human serum albumin (HSA), were immobilized on the assay surface and either detected by Raman scattering upon binding of GaM-IgG–conjugated SWNTs (GaM-IgG–SWNTs; using 785 nm excitation laser), or used in sandwich assays to capture analyte protein (e.g., anti-HSA IgG raised in mouse) from dilute serum (**Fig. 1b**).

To enhance Raman scattering intensity after direct or sandwich-assay detection of analyte by GaM-IgG–SWNT, we annealed the gold-coated substrate in a reducing hydrogen atmosphere to aggregate the gold film into particles (**Supplementary Fig. 2** online). Alternatively, a 5-nm layer of pure silver was deposited (**Supplementary Fig. 3** online) onto the assay surface. Both techniques reproducibly enhanced SWNT Raman signal ~60-fold without damaging SWNTs, as evidenced by the strong, characteristic SWNT radial breathing mode (< 500 cm^{-1}), longitudinal G^+ and transverse G^- mode (near 1,590 cm^{-1}) signals (**Fig. 1c**) observed uniformly over the substrate. The strong SERS effect was attributed to field enhancement by surface plasmons of metal particles, formed over the entire substrate in near-resonance with the 785-nm laser used for Raman scattering measurements (**Supplementary Fig. 4** online)[30]. For quantitative protein detection, the SWNT G-mode scattering intensity was used, as it demonstrates a high signal-to-noise ratio and very narrow peak width (~20 cm^{-1} FWHM)[31].

Selective and sensitive detection by SWNT Raman tags

The selectivity of a protein assay depends on both effective antibody conjugation and the minimization of nonspecific binding. We functionalized SWNTs with a 1:1 mole ratio mixture of 1,2-distearoyl-*sn*-glycero-3-phosphoethanolamine-coupled branched-methoxyPEG (DSPE-3PEO), which provided nonspecific binding resistance[11,27,32] (**Supplementary Fig. 5** online), and linear 1,2-distearoyl-*sn*-glycero-3-phosphoethanolamine carbamyl-PEG-amine (DSPE-PEG_{5000}-NH_2), which provided sites for bioconjugation. To evaluate the selectivity of this assay, we immobilized different proteins on PEGylated gold-coated glass substrates and tested them for binding with GaM-IgG–SWNTs through Raman detection (**Fig. 2a**). We observed specific GaM-IgG–SWNT binding only to the six mouse IgGs immobilized on the substrate, and not to the other eight negative-control protein spots (**Fig. 2b**). The application of SWNT Raman tags in biomolecule detection is highly generalizable to any system with adequate binding affinity and specificity. A summary of biomolecules used in SWNT Raman sensing and their affinities is provided in **Supplementary Table 1** online. In addition to Raman tags for protein assays, SWNTs have been used as tags for the *in vitro* Raman labeling of various cell membrane receptors[22,26,27,29,32]. These include both low- and high-affinity interactions, such as those between cyclic RGD peptide with the cell adhesion molecule $\alpha_v\beta_3$ integrin and anti-CD20 (Rituxan;

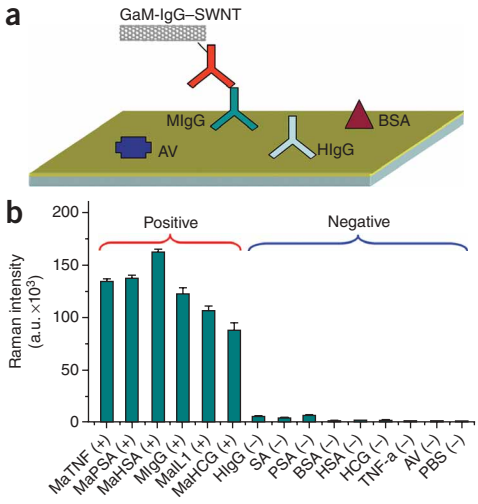

Figure 2 Highly selective recognition of surface-bound proteins by SWNT-antibody conjugates. (**a**) Two-layer, direct assay of mouse IgGs, which are immobilized with a complex set of protein analytes including BSA, human IgGs and avidin, arrayed on a gold-coated glass substrate by detecting GaM-IgG–SWNT Raman intensities. (**b**) G-mode intensities of GaM-IgG–SWNT conjugates bound to various protein spots on the substrate. Specific target proteins that were detected included polyclonal mouse (M)IgG, mouse anti-PSA (anti–prostate specific antigen), mouse anti-TNF (tumor necrosis factor), mouse aHSA, mouse aIL1 (anti interleukin-1) and mouse aHCG (anti–human chorionic gonadotropin). Negative control proteins included human IgG (HIgG), streptavidin (SA), PSA, BSA (bovine serum albumin), HSA, HCG, TNF, AV (avidin). PBS was also spotted on the surface as a control.

rituximab) with CD20, respectively. Examples of specific detection over a wide range of binding affinities are provided in **Supplementary Figures 6–9** online. These include SWNT Raman tags used to detect the interaction of streptavidin with biotin, DNA hybridization, the interactions of protein A and protein A/G with goat IgG and *in vitro* labeling of cell surfaces with cyclic RGD peptide.

To explore the sensitivity limit of SWNT Raman-based protein detection, we used HSA and GaM-IgG–SWNTs as model capture and reporting agents for sandwich-assay detection of monoclonal mouse anti-HSA IgG spiked into fetal bovine serum (FBS, **Fig. 1**). **Figure 3a** shows Raman mapping images of HSA spots after exposure to various concentrations of anti-HSA from 100 pM to 1 fM followed by incubation with GaM-IgG–SWNTs. The images were generated by plotting the integrated SWNT G-band intensity at each point (50 μm × 50 μm pixel size) over one quarter of the protein spot. In the maps, uniform SWNT signals were observed within HSA spots exposed to anti-HSA at concentrations > ~1 pM. At lower concentrations, the SWNT signal was sparse, consistent with a small number of anti-HSA

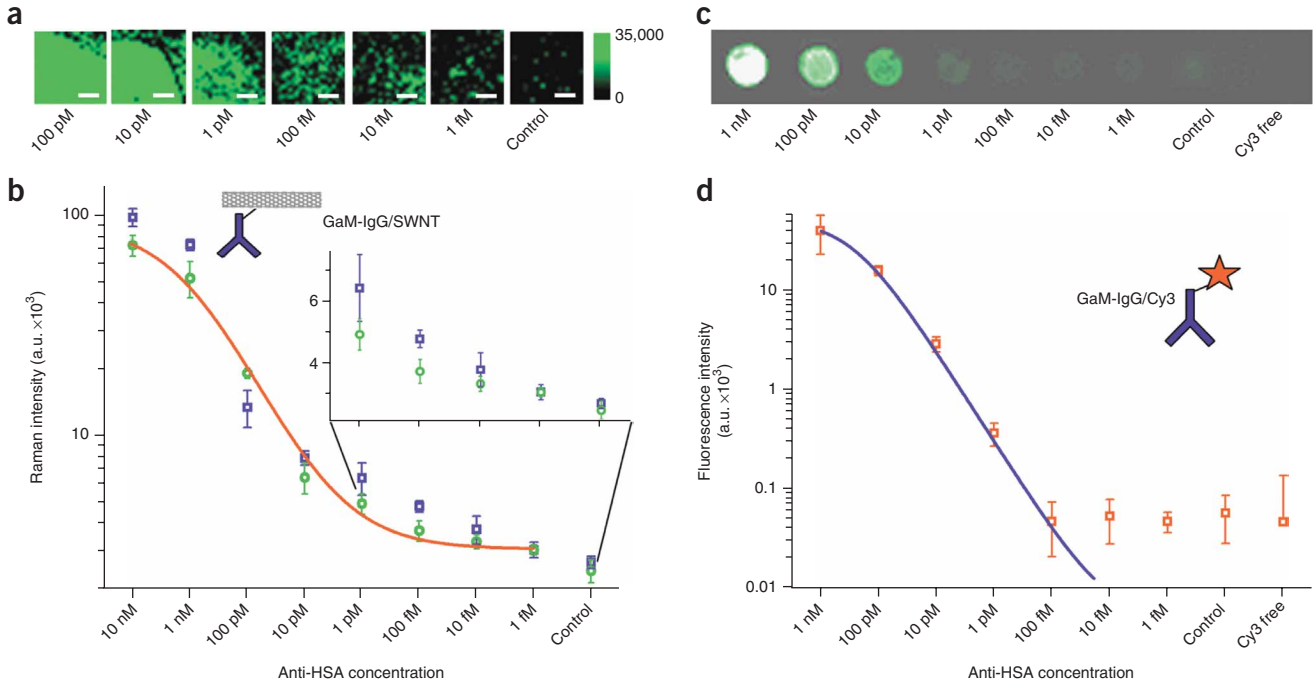

Figure 3 Femtomolar protein detection using SWNT Raman labels, compared with fluorescence-based protein microarray detection. (**a**) Raman mapping images showing integrated SWNT G-band peaks for model protein sandwich assays of anti-HSA in FBS ranging in concentration from 100 pM to 1 fM and an FBS control. Scale bar, 300 μm. (**b**) A log-log plot of the G-band Raman intensity versus anti-HSA concentration from two separate trials (blue and green), performed using different substrates and different GaM-IgG–SWNT conjugate batches on different days. A sigmoidal dependence was observed and fit by four-parameter logistic function (red curve). This suggests that protein quantification by Raman scattering of SWNT tags is limited by surface-receptor saturation and steric hindrance at high concentrations, and by residual nonspecific binding at the lower detection limit. Separate trials were performed using entirely different reagents, including different batches of GaM-IgG-SWNT and different gold-coated glass slides, performed on different days. (**c**) Fluorescence-based microarray detection of anti-HSA, depicted as GaM-IgG–cy3 fluorescence levels of HSA array spots exposed to anti-HSA, ranging in concentration from 1 nM–1 fM. The fluorescence of anti-HSA bound to HSA on the substrate was also recorded without exposure to GaM-IgG–cy3 as a measurement of autofluorescence and background noise. (**d**) Mean fluorescence versus analyte concentration from 1 nM to 1 fM. FBS-only and fluorophore-free controls are also included in the plot. Fluorescence observed for HSA array spots exposed to anti-HSA at concentrations <1 pM was not distinguishable from background fluorescence (without exposure to the cy3 fluorophore), indicating that sensitivity was limited by a poor signal-to-noise ratio.

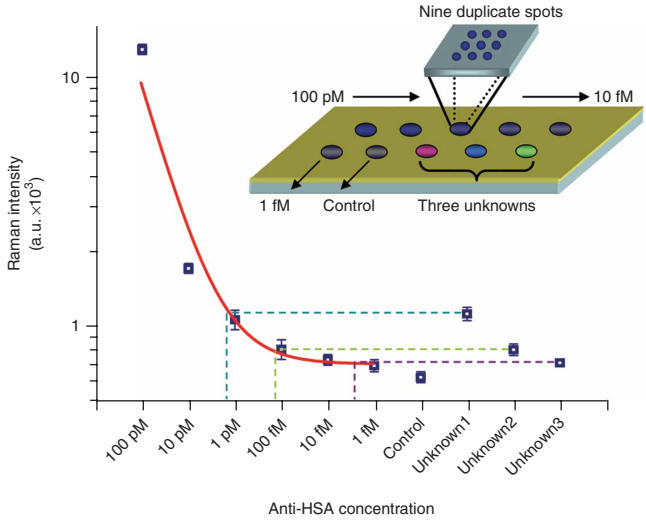

Figure 4 Calibration curve of mouse anti-human serum albumin measured in microarray format from nine duplicate protein spots at each analyte concentration by SWNT Raman tags. A limit of detection at 1 fM is observed with a dynamic range greater than six orders of magnitude. Four-parameter logistic function fitting of the data shows a sigmoidal dependence (red curve). Blind unknown analyte samples were prepared at 5 pM, 200 fM and 5 fM. Using the calibration curve, they were accurately quantified as 2 pM, 110 fM and 4 fM respectively.

IgGs captured by the HSA layer. Defining the limit of detection as twice the s.d. above the control (without analyte), we reproducibly obtained anti-HSA detection sensitivity down to 1 fM, over eight orders of dynamic range (**Fig. 3b**). The data exhibited sigmoidal or S-shape behavior[33]. This suggests saturation and steric hindrance effects for detection at high concentrations and increased the proportional influence of residual nonspecific binding effects at the lower detection limit.

To compare our SWNT-Raman-based detection to standard fluorescence-based protein microarray methods, we performed both assays in parallel. Protein microarray experiments were carried out on SuperEpoxide II slides by replacing the GaM-IgG–SWNT tags with cyanine-3 (cy3)-labeled GaM-IgG. A limit of detection of ~1 pM of anti-HSA was reproducibly obtained with arrayed fluorescence detection (**Fig. 3c,d** and **Supplementary Fig. 10** online), and this sensitivity limit was comparable to previous observations[1]. For fluorescence-based protein microarrays, we found that the fluorescence signals from HSA spots exposed to ≤100 fM analyte were similar to those measured at protein spots without any exposure to cy3-labeled GaM-IgG. This indicates that for detection of anti-HSA IgG concentrations ≤100 fM, fluorescence intensity was comparable to the background noise of substrates and reagent molecules, thus limiting the sensitivity to ~1 pM. Conversely, we observed no proteins or substrates exhibiting Raman peaks at the SWNT G-band position in control experiments (**Supplementary Fig. 11** online). Thus, reduced background contribution and an improved signal-to-noise ratio, resulting from bright Raman scattering spectra and surface-enhancement techniques, provide a broader dynamic range than fluorescence-based techniques. The sharp, surface-enhanced and background-free Raman scattering peaks observed in our detection method afforded ~1,000-fold improved sensitivity over fluorescence methods in this model-protein system.

The inflection point slope of the analyte-dependent dose-response curve is expected to be unity. This is nearly observed for the fluorescence-based assay of anti-HSA (slope of 0.88), whereas SWNT-Raman tags show an inflection point slope of 0.60. This deviation from theory may be due to nonlinear effects of surface-enhanced Raman scattering[34]. Despite such effects, the observation of sufficiently large Raman signal change down to 1 fM is noteworthy and can be used to measure low concentrations. Curve fitting is a

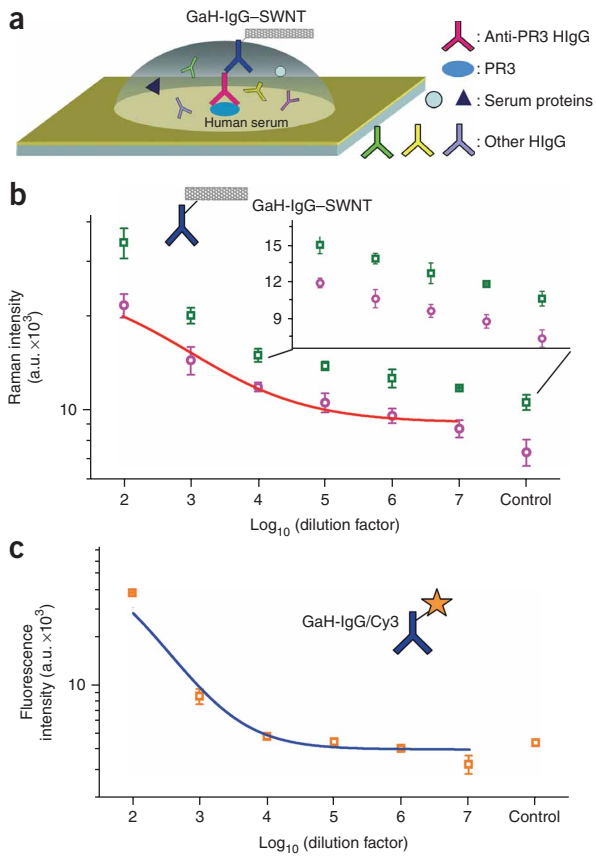

Figure 5 Raman versus fluorescence-based protein microarray detection of aPR3, a biomarker for Wegener's granulomatosis, in human serum. (**a**) Specific detection of aPR3 spiked into dilute human serum. Anti–proteinase 3 is captured by PR3 antigen on a PEGylated, gold-coated substrate, and detected by anti-human IgG conjugated SWNT Raman tags. (**b**) SWNT G-mode intensity as a function of aPR3 analyte concentration, captured from dilute human serum. The data show two separate sensing trials, using different assay substrates and different batches of GaH-IgG–SWNTs. Deviation in signal intensity is systematic, and likely a product of the deviation in the thickness of the gold film on the assay substrate and slight variation in the loading efficiency of anti-human IgG to the nanotube tags from batch to batch. Our assay design, like most bioassays, requires the use of simultaneous calibration curve measurements on the same chip. Accurate determination of unknown concentrations is possible because all measurements, standards and unknowns, are performed with the same reagents on the same assay substrate (e.g., **Fig. 4**). The observed sigmoidal dependence, fit by four-parameter logistic function (red curve) suggests that protein quantification by Raman scattering of SWNT tags is limited by surface-receptor saturation and steric hindrance at high concentrations, and by residual nonspecific binding at the lower detection limit. (**c**) Mean fluorescence as a function of aPR3 concentration captured from dilute human serum in a microarray experiment parallel to that described in **b**. A sigmoidal dependence, modeled by four-parameter logistic fit (blue curve), was observed.

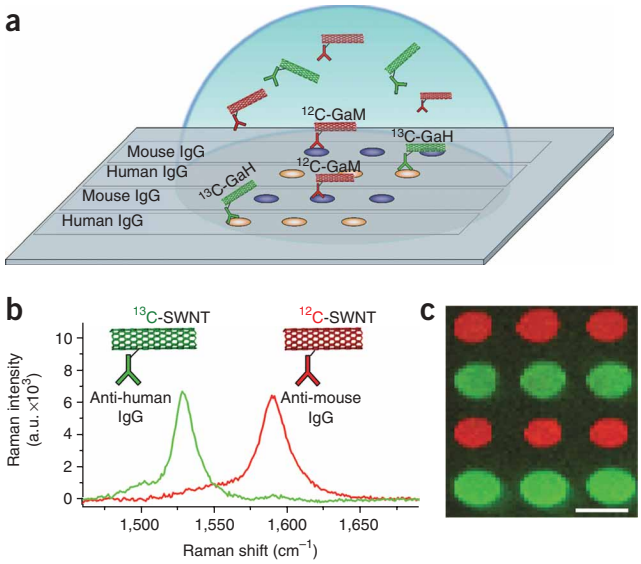

Figure 6 Multi-color SWNT Raman labels for multiplexed protein detection. (**a**) Two-layer, direct, microarray-format protein detection with distinct Raman labels based upon pure ^{12}C and ^{13}C SWNT tags. ^{12}C and ^{13}C SWNTs were conjugated to GaM and GaH-IgGs, respectively, providing specific binding to complimentary IgGs of mouse or human origin, even during mixed incubation with analyte (as shown). (**b**) G-mode Raman scattering spectra of ^{12}C (red) and ^{13}C (green) SWNT Raman tags are easily resolvable, have nearly identical scattering intensities, and are excited simultaneously with a 785 nm laser. This allows rapid, multiplexed protein detection. (**c**) Raman scattering map of integrated ^{12}C (red) and ^{13}C (green) SWNT G-mode scattering above baseline, demonstrating easily resolved, multiplexed IgG detection based upon multi-color SWNT Raman labels. Scale bar, 500 μm.

standard technique, which we used to quantify our data in this concentration region, and sigmoidal (four-parameter logistic) regressions have adequately fit the data and allowed quantification.

To exemplify this, we conducted a blind study in which three samples with unknown concentrations of anti-HSA were prepared and run in parallel with standards. Each data point value was determined by averaging nine duplicate microarray protein spots on the same assay substrate (**Fig. 4**). The average intensity was taken as the average of the individual mean scattering intensities ($n = 9$), and error bars were calculated from the s.d. between the mean scattering intensities of the nine duplicate spots. Such treatment yielded a calibration curve well fit by a logistic regression over six orders of magnitude (**Fig. 4**), along with mean scattering intensities for the three unknowns and an analyte-free control. Note that only six decades of analyte concentration were used for the calibration curve to avoid overcrowding of the substrate and possible cross-contamination. The three unknowns were prepared as 5 pM, 200 fM and 5 fM analyte solutions. Sensitivity down to the fM range was observed, within a factor of two to three. Experimental quantification of the three blind unknown analyte samples as 2 pM, 110 fM and 4 fM, respectively, demonstrates the accuracy of SWNT Raman tag detection despite nonlinear effects.

Highly sensitive autoimmune biomarker detection in human serum

We applied our SWNT Raman labels to clinically relevant detection related to Wegener's granulomatosis, an autoimmune disorder associated with anti-neutrophil cytoplasmic antibodies (cANCA)[35]. The disease is characterized by multi-organ vasculitis and can be fatal in severe cases. The positive predictive value of immunohistological staining, the gold standard for Wegener's granulomatosis diagnosis and treatment, is only ~50%[35]. Autoantibodies directed against proteinase 3 (PR3), which are directly implicated in the pathogenesis of the disease, are also used to diagnose Wegener's granulomatosis. Immunoassays for anti–proteinase 3 (aPR3) are more effective in prediction of Wegener's granulomatosis flares than staining alone[36]. We synthesized goat anti-human (GaH) secondary antibody Raman tags (GaH-IgG–SWNT) for detection of human aPR3 in human serum, mimicking the serum of a Wegener's granulomatosis-positive patient. A human IgG sample containing aPR3 isolated from a c-ANCA–positive individual was diluted at 1:10^2 to 1:10^7 in 1% normal human serum (**Fig. 5a**). A normal human serum sample, without spiked aPR3 (control), was included as a negative control. Detection of aPR3 by the SWNT Raman method in comparison with the negative control sample was successful over more than seven decades of dilution (**Fig. 5b**). A sigmoidal dependence, modeled by four-parameter logistic fit (blue curve) was observed, and the inflection point slope was ~0.50. Using cy3-labeled GaH-IgG, the limit of detection was reached at only four orders of dilution of the original aPR3–spiked human serum solution. Beyond that, the signals were comparable to the background noise, measured from the normal human serum control (**Fig. 5c**). A sigmoidal dependence was fit by four-parameter logistic function (red curve; inflection point slope ~0.90).

Multicolor detection by SWNT Raman tags

Our SWNT Raman labels can also be applied for multicolor detection. For this, we synthesized ^{12}C and ^{13}C isotopic SWNTs by chemical vapor deposition[37,38] using ^{12}C- and ^{13}C-pure methane, respectively. The Raman mode frequency scales with atomic mass as[39] $\omega \propto m^{-1/2}$. The G-band Stokes' shift of pure ^{13}C SWNTs (ω_{C13}) relates to that of pure ^{12}C SWNTs ($\omega_{C12} = 1{,}590$ cm^{-1}) by $\omega_{C13} = [1-(12/13)^{1/2}]\omega_{C12} = 1{,}528$ cm^{-1}, as observed experimentally (**Fig. 6**). By comparing the Raman scattering intensity of ^{12}C and ^{13}C SWNT G-bands at their respective maxima, ~0.5% cross-talk was observed for the isotopomers (**Supplementary Fig. 12** online). Through differential conjugation of minimally cross-reactive secondary IgGs, SWNTs could detect two types of IgGs simultaneously. GaM and GaH IgGs were conjugated to ^{12}C SWNTs (^{12}C-GaM) and ^{13}C SWNTs (^{13}C-GaH), respectively. A mixture of the two conjugates was incubated on the sensing assay surface, leading to differential binding to mouse and human primary IgGs with high selectivity (**Fig. 6c** and **Supplementary Fig. 13** online). More colors may be used by varying the ^{12}C/^{13}C ratio during growth (**Supplementary Fig. 14** online) or by monitoring the radial breathing modes of diameter-separated SWNTs[40,41]. This may enable multicolor SWNT tags to be used for multiplexed protein and biomarker assays[42].

DISCUSSION

We used SWNT Raman tags for highly selective and sensitive protein detection. Their high scattering cross-section, resonance-enhancement, simple spectra and facile isotopic tuning make SWNTs ideal Raman tags for sensitive detection of proteins and other biomolecules. The development of a branched-PEG coating, providing both amine functionality and inert methoxy termini on PEGylated SWNTs, enabled production of target-specific, biocompatible nanotubes with minimal nonspecific interactions between surfaces, proteins and SWNTs. Optimization of the SWNT-antibody conjugates was

especially challenging: other attempts at functionalization led to unacceptable nonspecific binding between proteins and nanotubes, and even small degrees of nonspecific binding prevented protein detection at the 1–100 fM level due to false signal.

The coupling of SERS-active gold or silver structures to SWNT Raman tags allowed increased signal-to-noise ratios for protein detection, reducing assay time and improving the limits of detection. The sharp SWNT Raman scattering peaks are not plagued by quenching close to metal surfaces, as is observed with typical fluorescent dyes. This enables microarrays to be performed on a variety of metal-coated substrates, using well-established surface chemistry for selective and sensitive protein detection.

Although our current method of SERS, involving the formation of random, nanoscopic metal clusters upon annealing or evaporation, allows limits of protein detection 1,000-fold lower than fluorescence-based methodologies, individual SWNT Raman tags bound to the same analyte array spot likely experience a range of scattering enhancement-factors. These depend on the location of nanotubes relative to metal structures, the local field enhancement of SERS hot spots and the spatial and statistical distribution thereof. Small numbers of the 'brightest' SERS hot spots exist. Thus, in a single spectral acquisition, SWNT Raman tags experiencing the greatest field enhancement may contribute to the majority of the total scattering intensity[34]. In SWNT-based protein detection, aggregation of a gold thin-film into nanostructures occurs after the statistical binding of IgG-SWNT tags to immobilized analyte. At relatively high concentrations, SWNTs occupy the small percentage of locations yielding the greatest surface enhancement (that is, saturation), thus contributing the majority of the total intensity in a nonlinear fashion. At reduced analyte concentrations, the spatial distribution of bound SWNT tags is too few to statistically occupy such hot spots. This leads to a proportionally increased contribution of less-enhanced SWNTs to the average intensity at each concentration. Such dependence generates a nonlinear relationship between sensitivity and analyte concentration.

Although SERS and saturation effects contribute to the nonlinearity of dose-response quantification, the observation of sufficiently large, surface-enhanced, Raman signal change down to 1 fM of model analyte is very important, owing to improved signal-to-noise ratios and reduced background interference. Logistic (four-parameter) curve-fitting enabled accurate quantification of unknown analyte samples, a model analyte and a serum biomarker of human disease.

In summary, we used antibody-tagged SWNTs as multi-color Raman labels to detect proteins in microarrays on various surfaces. The unique functionalization and bioconjugation chemistry of SWNTs, combined with protein immobilization on PEGylated, Raman-enhancing surfaces enabled us to apply the sharp, background-free Raman signatures of SWNTs to reproducible protein detection down to 1 fM (or 0.15 pg/ml) of analyte. This methodology was then applied to the clinically relevant detection of an autoimmune disease biomarker, aPR3 in native serum. In all cases, the detection limit of the SWNT Raman assay was three orders of magnitude better than standard fluorescence assays. Although this work focused on antibody-antigen interactions, the application of SWNT Raman tags in specific biomolecule targeting and detection should be equally applicable for probing protein-protein interactions and nucleic acid hybridization. Application of background-free, surface-enhanced, multicolor SWNT Raman labels may eventually enable simultaneous detection of multiple analytes in complex fluids, with 1 fM sensitivity in a multiplexed, arrayed fashion.

METHODS

SWNT-antibody conjugates. SWNTs in this study were either raw HipCO SWNTs (Carbon Nanotechnologies) or iron ruthenium bimetallic catalyzed[37] chemical vapor deposition SWNTs (^{12}C- and ^{13}C-methane[38] as the gas sources, respectively). Aqueous SWNT suspensions were prepared by 1 h bath sonication of an aqueous solution of a 1:1 mol ratio mixture of DSPE-3PEO, (M_n ~ 8,000) and DSPE-PEG$_{5000}$-NH$_2$ (M_n ~ 5,000) surfactants (NOF Corp.), as described previously[25,26,43].

To conjugate GaM-IgG or GaH-IgG (Pierce) to SWNTs, first Traut's Reagent (Pierce) was used to thiolate primary amines on the IgG. Sulfo-SMCC (sulfosuccinimidyl 4-*N*-maleimidomethyl cyclohexane-1-carboxylate, Pierce) was mixed at a 1:5 molar ratio with the SWNT suspension and incubated at pH 7.4 for 2 h at 22 °C. The excess sulfo-SMCC was then removed by centrifugal filtration through a 100-kDa molecular weight cutoff membrane (Millipore). After filtration, a tenfold molar excess of thiolated GaM-IgG (or GaH-IgG) was added into the SWNT suspension and reacted overnight in PBS at 4 °C. Excess unconjugated IgGs were removed by filtration. The antibody-conjugated, short SWNTs (50–150 nm long) were characterized by atomic force microscopy (Nanoscope IIIa, Veeco).

Protein arrays for Raman assay. Gold-coated (5 nm Au/0.2 nm Ti) glass slides were washed and oxygen plasma treated (Gabler Labor Instrument) and immersed into a 5 mM cysteamine (Aldrich) ethanol solution overnight. The substrate was then immersed for 2 h in a DMF solution containing 0.1 mM 6arm-PEG-COOH (M_n ~ 10,000, **Supplementary Methods** online), 50 mM 1-ethyl-3-(3-dimethylaminopropyl) carbodiimide hydrochloride (EDC, Aldrich) and 50 mM *N*-hydroxysuccinimide (NHS, Pierce) to form gold surfaces coated with branched PEG (**Supplementary Fig. 15** online). For specificity experiments, 0.5 µl of 1 µM solutions of polyclonal MIgG (Sigma), mouse anti–prostate-specific antigen (PSA, Fitzgerald), mouse anti–tumor necrosis factor (TNF, Pepro Tech), mouse anti-HSA (Medix MAB), mouse anti–interleukin-1 (IL-1, Fitzgerald), mouse anti–human chorionic gonadotropin (HCG, Biospacific), human IgG (Sigma), streptavidin (Pierce), PSA (Fitzgerald), BSA (Pierce), HSA (Sigma), HCG (Biospacific), TNF (Pepro Tech) and AV (Avidin, Sigma) were placed via pipette onto the EDC/NHS-activated branched PEG surface and incubated for 2 h in PBS at pH 7.2. PBS (Fisher) was also spotted on the surface as a control. For concentration-dependent sensitivity experiments, 0.5 µl of 1 µM protein (e.g., HSA or PR3) solution was spotted via pipette and incubated on the EDC/NHS-activated branched-PEG coating for 2 h in PBS at pH 7.2. The substrates were immersed in 0.1 M Tris in PBS solution for 1 h to quench the reaction. The substrates were then immersed into 3% FBS and 0.5% wt/vol Tween-20 (Aldrich) PBS solution overnight at 4 °C for blocking. For multi-color Raman detection, 1 µM purified human IgG and mouse IgG were printed in two sets each of triplicate 400 µm diameter protein spots via solid printing pins (Array-It) with the robotic Bio-Rad VersArray Compact array printer on Superfrost Plus glass slides (Fisher) at 25 °C and 65% humidity.

Protein Raman detection. For two-layer direct detection of immobilized proteins (**Fig. 2**), 20 nM GaM-IgG–SWNT in PBS (molar extinction coefficient of short SWNTs[44] $\varepsilon_{808nm} \approx 0.0079$ nM^{-1}cm^{-1}) solution was incubated on the surface for 30 min to allow binding before Raman detection. For sandwich detection of anti-HSA, eight anti-HSA solutions (10 nM–1 fM in 3% FBS/PBS) were incubated on the substrate containing an array of HSA spots (as described above) for 24 h at 4 °C. A 3% FBS/PBS solution without anti-HSA was incubated with an HSA protein spot and served as an analyte-free control. A hydrophobic PAP (Pen/liquid blocker) (Cedarlane Labs) was used to circumscribe the array before incubation. After soaking the assay substrate in PBS for 5 min and gently rinsing with PBS and water, 20 nM GaM-IgG–SWNT solution was incubated above captured analyte for 30 min at 22 °C. For aPR3 detection, all aPR3 (Immunovision) solutions were prepared by spiking analyte into 1% normal human serum and 3% FBS in PBS. The total human IgG content in the original aPR3–containing sample, determined by ELISA, was 17 mg/ml. Ten serially diluted aPR3 serum solutions, as well as an aPR3–negative, dilute normal human serum sample, were incubated on PR3 spots for 24 h at 4 °C. We then incubated 20 nM GaH-IgG–SWNT conjugates on the spots, allowing binding before Raman detection.

For SERS, assays on gold substrates were annealed in protective hydrogen gas at 400 °C for 3 min to form gold clusters over the substrates, which enhanced the SWNT Raman signals. Alternatively, for assays on glass substrates, as in the multi-color experiments, SERS was carried out by depositing a 5 nm thick silver film on the substrate by electron beam evaporation. Silver clusters were formed over the entire substrate, coating the intact proteins and SWNT tags. All Raman spectra were collected on a Renishaw micro-Raman instrument (laser excitation wavelength at 785 nm). A 20× objective lens (Leica) was used to focus on the protein spots. A laser spot of ~200 μm^2 was used during the Raman scattering measurements. At each protein spot, at least 20 spectra were recorded at different spatial points to obtain an averaged SWNT Raman scattering intensity, as well as the s.d., depicted as error bars. The collection time for each spectrum was 1 s. For Raman imaging of protein array spots (**Fig. 3a**), Raman mapping was carried out using a 20× objective, and the integrated G-band intensity was measured over the whole protein spot (~3 mm^2), pixel by pixel (pixel size 50 μm × 50 μm). Error bars for map analyses were generated as the s.d. of the means of duplicated assay spots ($n = 9$).

^{12}C and ^{13}C SWNT direct IgG detection assay. A solution comprising a mixture of ~5 nM ^{12}C GaM-IgG–SWNT and ~5 nM ^{13}C GaH-IgG–SWNT conjugates in PBS was incubated over robotically printed polyclonal mouse and human IgG spots on Superfrost Plus glass slides for 30 min at 22 °C. After silver deposition, mapping of the SWNT G band intensity over the 2 mm × 3 mm area was performed with 30 μm steps in x and y. The mouse IgG and human IgG map image was generated by integration of the respective G-bands of ^{12}C and ^{13}C SWNTs above background, and plotted as false-colored maps (**Fig. 6c**).

Standard fluorescence-based protein microarray assay. For fluorescence-based[16] anti-HSA and aPR3 detection, arrays of six duplicate protein spots were printed robotically. HSA was printed at 1 μM in PBS on Super-Epoxide 2 slides (Array-It), and PR3 was printed at 0.2 mg/ml in PBS onto nitrocellulose-coated FAST slides (Whatman). Arrays were blocked for 1 h at 22 °C in PBS with 0.05% Tween-20 and 3% FBS, and then incubated for 3–24 h at 4 °C with the indicated dilutions of anti-HSA (in 3% FBS/PBS) or aPR3 (in 1% human serum and 3% FBS/PBS), in addition to unspiked serum controls. After washing, arrays were incubated with 400 μl of a 10 pM solution of GaM-IgG–cy3 or GaH-IgG–cy3 in PBS for 1 h at 22 °C in the dark[16]. The slides were scanned using a GenePix 4000B Scanner (Axon Labs) with a 17 mW, 532 nm excitation laser and photo-multiplier tube gain set to 400 for nitrocellulose-coated FAST slides and 800 for Super-Epoxide 2 Slides. Array spot features were automatically selected at 10 μm pixel resolution by GenePix Pro 6.0 software (Axon Labs). Reported fluorescence values were calculated as the local background corrected (**Supplementary Methods**) mean of all pixels identified as array features for each analyte dilution point. Error bars represent the s.d. between duplicate spots from the same assay substrate.

Note: Supplementary information is available on the Nature Biotechnology website.

ACKNOWLEDGMENTS

This work was supported by the National Institutes of Health/National Cancer Institute–funded Center for Cancer Nanotechnology Excellence Focused on Therapeutic Response U54 CA119367 at Stanford University, and NIH-NCI R01 CA135109-01. The authors would like to thank Nozomi Nakayama-Ratchford and Sarunya Bangsaruntip for their assistance in developing carbon nanotube–protein conjugates.

AUTHOR CONTRIBUTIONS

Z.C. and S.M.T. contributed equally to the work, developing the SWNT passivation and conjugation schemes presented, as well as the procedure for obtaining SERS-active surfaces and the related protein immobilization methodology. A.P.G. contributed synthesis of 6-arm branched carboxy-PEG. M.G.K. and P.J.U. contributed to fluorescence-based detection of anti-proteinase 3. D.D. and Z.L. contributed by assisting in preparing SWNT-antibody and SWNT-peptide conjugates. X.W. and G.Z. contributed by assisting in the preparation of SERS-active substrates. X.L., K.J. and S.F. contributed by providing isotopomer SWNTs. H.D. designed the research and contributed much direction and assistance to this project.

Published online at http://www.nature.com/naturebiotechnology/
Reprints and permissions information is available online at http://npg.nature.com/reprintsandpermissions/

1. Bailey, R.C., Kwong, G.A., Radu, C.G., Witte, W.N. & Heath, J.R. DNA-encoded antibody libraries: a unified platform for multiplexed cell sorting and detection of genes and proteins. *J. Am. Chem. Soc.* **129**, 1959–1967 (2007).
2. Hayes, F.J., Halsall, H.B. & Heineman, W.R. Simultaneous immunoassay using electrochemical detection of metal ion labels. *Anal. Chem.* **66**, 1860–1865 (1994).
3. Landry, J.P., Zhu, X.D. & Gregg, J.P. Label-free detection of microarrays of biomolecules by oblique-incidence reflectivity difference microscopy. *Opt. Lett.* **29**, 581–583 (2004).
4. Wegner, G.J., Lee, H.J. & Corn, R.M. Characterization and optimization of peptide arrays for the study of epitope-antibody interactions using surface plasmon resonance imaging. *Anal. Chem.* **74**, 5161–5168 (2002).
5. Cao, Y.C., Jin, R., Nam, J.M., Thaxton, C.S. & Mirkin, C.A. Raman dye-labeled nanoparticle probes for proteins. *J. Am. Chem. Soc.* **125**, 14676–14677 (2003).
6. Li, T., Guo, L. & Wang, Z. Microarray based Raman spectroscopic detection with gold nanoparticle probes. *Biosens. Bioelectron.* **23**, 1125–1130 (2008).
7. Grubisha, D.S., Lipert, R.J., Park, H.Y., Driskell, J. & Porter, M.D. Femtomolar detection of prostate-specific antigen: an immunoassay based on surface-enhanced Raman scattering and immunogold labels. *Anal. Chem.* **75**, 5936–5943 (2003).
8. Wu, G. *et al.* Bioassay of prostate-specific antigen (PSA) using microcantilevers. *Nat. Biotechnol.* **19**, 856–860 (2001).
9. Goldman, E.R. *et al.* Conjugation of luminescent quantum dots with antibodies using an engineered adaptor protein to provide new reagents for fluoroimmunoassays. *Anal. Chem.* **74**, 841–847 (2002).
10. Nam, J.M., Thaxton, C.S. & Mirkin, C.A. Nanoparticle-based bio-bar codes for the ultrasensitive detection of proteins. *Science* **301**, 1884–1886 (2003).
11. Chen, R.J. *et al.* An investigation of the mechanisms of electronic sensing of protein adsorption on carbon nanotube devices. *J. Am. Chem. Soc.* **126**, 1563–1568 (2004).
12. Kong, J. *et al.* Nanotube molecular wires as chemical sensors. *Science* **287**, 622–625 (2000).
13. Zheng, G., Patolsky, F., Cui, Y., Wang, W.U. & Lieber, C.M. Multiplexed electrical detection of cancer markers with nanowire sensor arrays. *Nat. Biotechnol.* **23**, 1294–1301 (2005).
14. MacBeath, G. & Schreiber, S.L. Printing proteins as microarrays for high-throughput function determination. *Science* **289**, 1760–1763 (2000).
15. Hudson, M.E., Pozdnyakova, I., Haines, K., Mor, G. & Snyder, M. Identification of differentially expressed proteins in ovarian cancer using high-density protein microarrays. *Proc. Natl. Acad. Sci. USA* **104**, 17494–17499 (2007).
16. Robinson, W.H. *et al.* Autoantigen microarrays for multiplex characterization of autoantibody responses. *Nat. Med.* **8**, 295–301 (2002).
17. Song, S. *et al.* A cancer protein microarray platform using antibody fragments and its clinical applications. *Mol. Biosyst.* **3**, 151–158 (2007).
18. Espina, V. *et al.* Protein microarray detection strategies: focus on direct detection technologies. *J. Immunol. Methods* **290**, 121–133 (2004).
19. Hartwell, L., Mankoff, D., Paulovich, A., Ramsey, S. & Swisher, E. Cancer biomarkers: a systems approach. *Nat. Biotechnol.* **24**, 905–908 (2006).
20. Jensen, L. & Schatz, G.C. Resonance Raman scattering of rhodamine 6G as calculated using time-dependent density functional theory. *J. Phys. Chem. A* **110**, 5973–5977 (2006).
21. Baughman, R.H., Zakhidov, A.A. & de Heer, W.A. Carbon nanotubes–the route toward applications. *Science* **297**, 787–792 (2002).
22. Heller, D.A., Baik, S., Eurell, T.E. & Strano, M.S. Single-walled carbon nanotube spectroscopy in live cells: towards long-term labels and optical sensors. *Adv. Mater.* **17**, 2793–2799 (2005).
23. Sun, Y.P., Fu, K.F., Lin, Y. & Huang, W.J. Functionalized carbon nanotubes: properties and applications. *Acc. Chem. Res.* **35**, 1096–1104 (2002).
24. Bahr, J.L. & Tour, J.M. Covalent chemistry of single-wall carbon nanotubes. *J. Mater. Chem.* **12**, 1952–1958 (2002).
25. Kam, N.W.S., Liu, Z. & Dai, H.J. Functionalization of carbon nanotubes via cleavable disulfide bonds for efficient intracellular delivery of siRNA and potent gene silencing. *J. Am. Chem. Soc.* **127**, 12492–12493 (2005).
26. Liu, Z. *et al. In vivo* biodistribution and highly efficient tumor targeting of carbon nanotubes in mice. *Nat. Nanotechnol.* **2**, 47–52 (2007).
27. Chen, R.J. *et al.* Noncovalent functionalization of carbon nanotubes for highly specific electronic biosensors. *Proc. Natl. Acad. Sci. USA* **100**, 4984–4989 (2003).
28. Schipper, M.L. *et al.* A pilot toxicology study of single-walled carbon nanotubes in a small sample of mice. *Nat. Nanotechnol.* **3**, 216–221 (2008).
29. Welsher, K. & Liu, Z. Daranciang & Dai, H.J. Selective probing and imaging of cells with single walled carbon nanotubes as near-infrared fluorescence molecules. *Nano Lett.* **8**, 586–590 (2008).
30. Nie, S. & Emory, S.R. Probing single molecules and single nanoparticles by surface-enhanced Raman scattering. *Science* **275**, 1102–1106 (1997).
31. Kneipp, K., Kneipp, H. & Kneipp, J. Surface-enhanced Raman scattering in local optical fields of silver and gold nanoaggregates - from single-molecule Raman spectroscopy to ultrasensitive probing in live cells. *Acc. Chem. Res.* **39**, 443–450 (2006).
32. Shim, M., Kam, N.W.S., Chen, R.J., Li, Y. & Dai, H.J. Functionalization of carbon nanotubes for biocompatibility and biomolecular recognition. *Nano Lett.* **2**, 285–288 (2002).

33. Diamandis, E.P. & Christopoulos, T.K. *Immunoassay* (Academic Press, San Diego, 1996).
34. Fang, Y., Seong, N.H. & Dlott, D.D. Measurement of the distribution of site enhancement in surface-enhanced Raman scattering. *Science* **321**, 388–392 (2008).
35. Jenne, D.E., Tschopp, J., Lüdemann, J., Utecht, B. & Gross, W.L. Wegener's autoantigen decoded. *Nature* **346**, 520 (1990).
36. Seo, P. & Stone, J.H. The antineutrphil cytoplasmic antibody-associated vasculitides. *Am. J. Med.* **117**, 39–50 (2004).
37. Li, X. *et al.* Selective synthesis combined with chemical separation of single-walled carbon nanotubes for chirality selection. *J. Am. Chem. Soc.* **129**, 15770–15771 (2007).
38. Liu, L. & Fan, S.S. Isotope labeling of carbon nanotubes and formation of ^{12}C-^{13}C nanotube junctions. *J. Am. Chem. Soc.* **123**, 11502–11503 (2001).
39. Ferraro, J.R., Nakamoto, K. & Brown, C.W. *Introductory Raman Spectroscopy* edn. 2 (Academic Press, San Diego, 2003).
40. Arnold, M.S., Green, A.A. & Hulvat, J.F. Stupp. S.I. & Hersam, M.C. Sorting carbon nanotubes by electronic structure using density differentiation. *Nat. Nanotechnol.* **1**, 60–65 (2006).
41. Tu, X. & Zheng, M. A DNA-based approach to the carbon nanotube sorting problem. *Nano. Res.* **1**, 185–194 (2008).
42. Liu, Z. *et al.* Multiplexed mutli-color Raman imaging of live cells with isotopically modified single walled carbon nanotubes. *J. Am. Chem. Soc.* doi:10.1021/ja806242t (20 September 2008).
43. Liu, Z. *et al.* Circulation and long-term fate of functionalized, biocompatible single-walled carbon nanotubes in mice probed by Raman spectroscopy. *Proc. Natl. Acad. Sci. USA* **105**, 1410–1415 (2008).
44. Kam, N.W.S., Connell, M.O., Wisdom, J.A. & Dai, H.J. Carbon nanotubes as multifunctional biological transporters and near-infrared agents for selective cancer cell destruction. *Proc. Natl. Acad. Sci. USA* **102**, 11600–11605 (2005).